Atomistic simulations of biologically realistic transmembrane potential gradients

Jonathan N. Sachs
Department of Molecular Biophysics and Biochemistry, Yale University, New Haven, Connecticut 06520

Paul S. Crozier
Department of Computational Materials and Molecular Biology, Sandia National Laboratories, Albuquerque, New Mexico 87185-1110

Thomas B. Woolf
Department of Physiology, The Johns Hopkins University School of Medicine, Baltimore, Maryland 21205

(Received 30 July 2004; accepted 7 October 2004)

We present all-atom molecular dynamics simulations of biologically realistic transmembrane potential gradients across a DMPC bilayer. These simulations are the first to model this gradient in all-atom detail, with the field generated solely by explicit ion dynamics. Unlike traditional bilayer simulations that have one bilayer per unit cell, we simulate a 170 mV potential gradient by using a unit cell consisting of three salt-water baths separated by two bilayers, with full three-dimensional periodicity. The study shows that current computational resources are powerful enough to generate a truly electrified interface, as we show the predicted effect of the field on the overall charge distribution. Additionally, starting from Poisson's equation, we show a new derivation of the double integral equation for calculating the potential profile in systems with this type of periodicity.
 [DOI: 10.1063/1.1826056]

INTRODUCTION

High-resolution structures of ion channels now enable understanding and modeling of membrane excitability on an atomic level.[1] The connection between ion channel structure and function fundamentally relies upon the transmembrane potential gradient, which drives channel gating and ion permeation.[2,3] The transmembrane potential is generated by (1) charge imbalance across the bilayer due to anion and cation populations, (2) charges in the lipid headgroups (zeta potential), and (3) ordering of partial charges and waters within the bilayer (dipole potential).[4] Experimental approaches give macroscopic information about these three components, via patch-clamp,[5] electrophoretic mobility,[6] and voltage-sensitive dyes[4] respectively. The microscopic functional form and atomic-level origins of the potential have been elusive due to the limited resolution of these available experimental techniques. Thus, theoretical and computational models that can reveal such detailed descriptions are desired.

All-atom molecular dynamics (MD) simulations have been used successfully to study details of interactions between ions and ion channels[7–9] and between ions and bilayers.[10–14] But because of limitations in the time- and length-scales accessible to all-atom simulations, MD has not been used to explicitly model the transmembrane potential gradient. Biologically relevant potential gradients are on the order of 100 mV, corresponding to a small asymmetric build-up of ions in the interfacial regions of the two monolayer leaflets of a lipid bilayer (on the order of 1 excess ion/10^4 Å^2 of bilayer).[15] An all-atom representation of this ion-:lipid ratio requires on the order of 10^5 atoms, historically too many. This limitation led to the development of implicit representations of both the transmembrane potential and the membrane itself, which have reduced number of atoms. In one important example, the Poisson–Boltzmann equation was modified to include the effect of a potential and used to calculate the charge distribution in the continuum and the electric field in the pore of an ion channel.[15,16] Another approach that avoids the need for huge bilayers has been to include an additional term in the MD force function, to account for the potential.[17,18] As with the continuum methods, this approach has relied upon a dielectric description of membrane (ϵ=2) and water (ϵ=80) in setting the position-dependent strength of the applied field.

In addition to the problem of limited simulation size, the need for periodic boundary conditions is a major hurdle to all-atom simulations of the transmembrane potential. Because simulations that employ electrostatic cut-offs suffer from well-known artifacts,[19–21] most modern simulations apply the Ewald summation technique for calculating long-range electrostatic interactions.[22] One requirement of the traditional Ewald sum is that the system must be periodically replicated in all three dimensions, including the one normal to the bilayer and parallel to the potential gradient. In order to establish and equilibrate a potential gradient, the salt-water baths on opposite sides of the bilayer (carrying the charge imbalance) cannot be connected periodically, as is the case in the traditional unit cell used for all-atom bilayer simulations. A similar problem has been addressed in simulations of salt-water embedded between oppositely charged electrodes.[23–27] An Ewald sum that eliminates the need for periodicity in one dimension can be used for long-range electrostatic calculations,[28–30] but the computational implementation is prohibitively slow.[25,31,32] An alternative is to modify

TABLE I. Number of ions in the starting configuration for each of the three salt-water baths shown in Fig. 1. In each case the concentration is 1 M, with the central region having 1 excess Na^+ and each of the two periodically connected outer regions having 0.5 excess Cl^- ions on average.

Simulation	Bath 1	Bath 2	Bath 3
Neutral	60 Na^+, 60 Cl^-	120 Na^+, 120 Cl^-	60 Na^+, 60 Cl^-
Electrified	60 Na^+, 60 Cl^-	121 Na^+, 120 Cl^-	60 Na^+, 61 Cl^-

the three dimensional Ewald sum and diminish the periodic interactions between the two salt-water baths by separating them with vacuum regions.[26] This method has been used recently in models of bilayer concentration gradients[33] and in an all-atom ion channel simulation.[34]

A straightforward solution to the periodicity problem is to simulate more than one bilayer per unit cell, but until now this has been considered too computationally expensive. Here, we take this approach, which allows for full three-dimensional periodicity and an all-atom representation of the transmembrane potential with no continuum approximations. Specifically, we simulate a system with three salt-water baths separated by two bilayers. The central salt-water bath carries a net charge of $+1$ e, while the two outer water baths, connected periodically, each carry on average a net charge of -0.5 e, hence eliminating the periodicity problem. We show a 170 mV potential gradient that, on a 10 ns time scale, affects the charge distribution in the entire system. A simulation with no potential gradient is also presented as a baseline for comparison. This approach is consistent with a recent simulation of a model membrane.[35] We also derive a double integral equation from Poisson's equation for calculating the potential profile in systems with this type of periodicity.

METHODS

Two double-bilayer systems were built using the CHARMM molecular mechanics package,[36] one with a charge imbalance due to excess ions (electrified) and one with no such imbalance (neutral). Details of the ion distributions are given in Table I and Fig. 1 shows a snapshot from the electrified simulation. Proceeding from the left-most point, there is an outer salt-water bath (-0.5 e), a bilayer (outer and then inner monolayer), a central salt-water bath ($+1.0$ e), a second bilayer (inner then outer monolayer) and finally a second outer water bath (-0.5 e). The initial configuration had one excess Na^+ in the central salt-water bath, and one excess Cl^- in the right-most salt-water bath. The system was built to optimize the trade-off between system size and a realistic potential drop. The voltage drop was predicted based upon the relation $V=Q/C$, where Q is the net charge per unit area and C is the capacitance, taken as 1 μF/cm^2, a common value used for lipid membranes.[15] The system consists of a total of 512 lipids, each of 4 monolayers having 128 lipids. Given the experimentally determined[37] area per lipid of 59.7 Å^2, the charge imbalance of $+0.5$ e/bilayer was predicted to produce a potential gradient of approximately 210 mV. Based on previous simulations[10,14] the length of the salt-water baths was set greater than the expected extent of salt-induced water ordering in the bilayer-electrolyte interface. The final dimensions were $87\times87\times120$ Å. Na^+ and Cl^- ions were added at random locations, each replacing a water molecule, to a final concentration of 1 M. This relatively high salt concentration was chosen to maximize the sampling of the ions as has been done previously.[10,14]

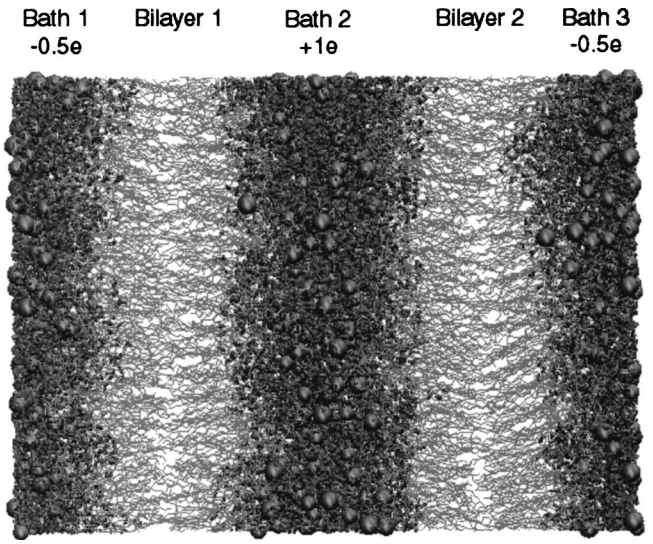

FIG. 1. Snapshot from the 170 mV simulation showing the three regions of salt-water separated by the two bilayers. The left and right edges are connected by periodic boundary conditions. There is an excess of 1 Na^+ in the central bath and 1 Cl^- in the two outer baths combined. The ions are represented as oversized spheres.

We performed all-atom molecular dynamics simulations of the constructed ensembles using the CHARMM22 force field[38,39] in the 2003 version of the large-scale atomic/molecular massively parallel simulator (LAMMPS), which is distributed freely as open-source software under the GNU Public License.[40–42] Bonds involving hydrogen atoms were held rigid using the SHAKE algorithm to enable a 2 femtosecond time step. The TIP3P waters were also held rigid by SHAKE. Each system was simulated at constant lipid bilayer surface area, but the simulation cell length in the z-direction was allowed to fluctuate in order to maintain isobaric conditions. A Nosé–Hoover thermostat/barostat was used to hold the simulations near 298 K and 1 atm. The z-direction box length stayed near 120 Å, with minor fluctuations, for both the neutral and the electrified system simulations.

Long-range electrostatics were computed using the particle-particle/particle-mesh (P^3M) method, which is very similar to the commonly-used particle mesh Ewald (PME) method, and has been shown to be slightly more efficient than PME.[43] We used a real-space cutoff of 10 Å, with a real-space/reciprocal-space partitioning parameter chosen for optimal speed given a desired level of accuracy.[44] The van der Waals (vdW) interactions were smoothly switched to zero between 8 and 10 Å.

Simulation of the neutral system was performed at Sandia National Laboratories on the large-scale Computational Plant (Cplant) cluster.[45] Each Cplant node is a 466 MHz 21264 (EV6) microprocessor. We were able to achieve a speed of approximately 0.3 ns of simulated time per day of compute time running in parallel on 64 processors of Cplant.

The 5-ns, 2.5 million time step simulation required 18 CPU days, scattered across a month of real time, including down time. Simulation of the electrified system was performed on Sandia's Institutional Computing Cluster (ICC). Each of the ICC nodes is a dual 3.06 GHz Xenon processor. We reached a simulation speed of 0.6 nanoseconds/day running in parallel on 20 of the dual processor ICC nodes. The 10-ns, 5 million time step simulation also required 18 CPU days during a month of real time.

We now derive a new form of Poisson's equation for calculating the electrostatic potential profile in our system with its unique boundary conditions. Taking Poisson's equation,

$$\frac{d^2\phi}{dz^2} = -\frac{1}{\epsilon_o}\sum_i q_i\rho_i(z), \tag{1}$$

where ϕ is the potential, ϵ_o is the permittivity constant, q_i is the charge on atom i, ρ_i is the density of atoms of type i, and z is the direction perpendicular to the membrane, we have a relationship between the equilibrium charge distribution and the potential field. Poisson's equation can be integrated twice, and the proper boundary conditions applied, in order to produce an equation that yields the potential profile as a function of z. After integrating twice, we have

$$\phi(z) = -\frac{1}{\epsilon_o}\sum_i q_i\int_0^z\int_0^s \rho_i(u)du\,ds + C_1 z + C_2, \tag{2}$$

where u and s are dummy variables, C_1 and C_2 are constants of integration. We switch the order of integration to get

$$\phi(z) = -\frac{1}{\epsilon_o}\sum_i q_i\int_0^z\int_u^z \rho_i(u)ds\,du + C_1 z + C_2. \tag{3}$$

Now, performing the inner integral, we obtain

$$\phi(z) = -\frac{1}{\epsilon_o}\sum_i q_i\int_0^z (z-u)\rho_i(u)du + C_1 z + C_2. \tag{4}$$

Since all simulations in this work have been done with periodic boundary conditions (PBC), we apply PBC, requiring that $\phi(0)=\phi(L)$, where L is the simulation box length in the z-direction. In addition, we arbitrarily choose $z=0$ as the reference point and set $\phi\,(0)=0$. Applying these conditions, C_2 becomes 0, and

$$C_1 = \frac{1}{\epsilon_o L}\sum_i q_i\int_0^L (L-u)\rho_i(u)du. \tag{5}$$

Finally, we have

$$\phi(z) = -\frac{1}{\epsilon_o}\sum_i q_i\left[\int_0^z (z-u)\rho_i(u)du - \frac{z}{L}\int_0^L (L-u)\rho_i(u)du\right]. \tag{6}$$

In practice, atomic charges are accumulated in narrow bins ($\Delta z \sim 0.1$ Å) positioned along the z-axis, perpendicular to the membrane surface. Snapshots of the dynamic system taken at 1 ps intervals provide a time-averaged net charge for each bin. A potential profile that is representative of the equilibrium state of the given system is then obtained by summing up the bins using Eq. (6).

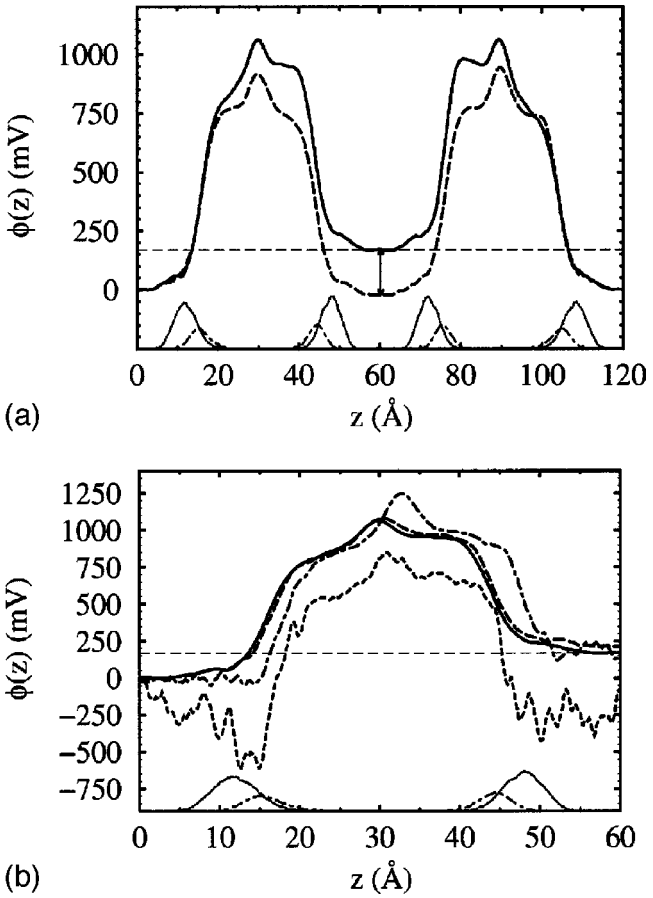

FIG. 2. Transmembrane potential profiles. (a) The profile from the neutral (long-dashed line) and 170 mV simulations (solid line) across the entire 120 Å system shown in Fig. 1 (0 Å, the left-most point, 120 Å, the right-most point). Vertical arrow highlights the difference in potential gradient between the two simulations. (b) Temporal build-up of the equilibrated potential profile. Symmetrized half-cell profiles from the 170 mV simulation extracted from the first 1 ps (dashed), 10 ps (dot-dashed), 1 ns (long dashed) and 10 ns (solid). Arbitrarily scaled density profiles for the lipid phosphate (dotted) and carbonyl groups (dot-dashed) from the electrified simulation are given at the bottom of both plots for spatial reference.

RESULTS AND DISCUSSION

Figure 2 demonstrates the basic aim of this study: Electrified bilayers can now be simulated with the multilayer method. The electrostatic potential profiles from both the neutral and electrified bilayer simulations, as calculated from Eq. (6), are given in Fig. 2(a). The most important feature is a potential gradient of 170 mV across both of the bilayers in the electrified simulation. Additionally, the shape of the profile in the electrified simulation is consistently different when comparing the outer and inner monolayers within each bilayer, reflecting their exposure to opposite ends of the electrical gradient. The significant changes in the center of the bilayers reflect the impact of the electrical gradient on the dipolar orientations of the hydrocarbon chains, and hence the dipole potential as described above. These differences are diminished in the neutral case, as would be expected. Com-

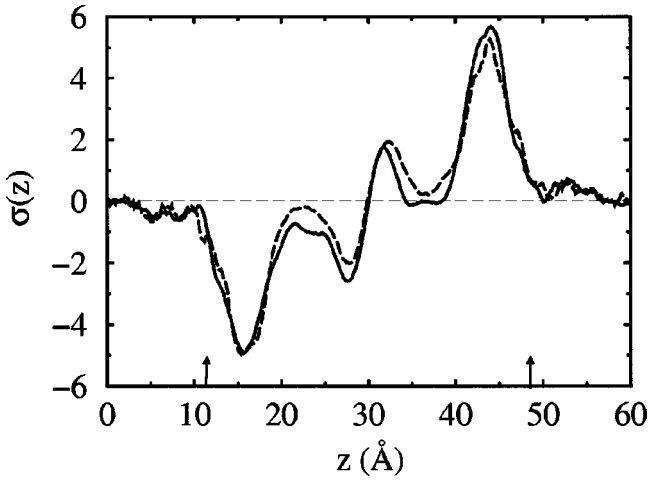

FIG. 3. Single integral, σ, of the symmetrized charge density from the neutral (long-dashed line) and 170 mV (solid line) simulations, showing the build-up of negative charge on the outer-most monolayer leaflets ($z<30$ Å), and positive charge on the innermost leaflets ($z>30$ Å) as predicted. Arrows indicate the peaks in the phosphate distributions given in Fig. 2.

paring the two simulations, it is not until deep within the lipid headgroup region (at approximately the level of the carbonyl groups) that the two profiles begin to diverge. The two potential profiles are identical in both of the outer salt-water baths, and level off in all three of the salt-water baths, showing that the simulation dimensions are large enough to accommodate the potential drop and charge screening.

The equilibration of the potential profile is of central concern in evaluating this multi-layer method for simulating transmembrane potential gradients. Figure 2 suggests that the relatively short timescale of these simulations is sufficient for the equilibration of the potential profile. In both simulations the profiles across the two bilayers are nearly identical, though there are some subtle variations deep within the hydrocarbon regions. To minimize the size of the simulations and still achieve a potential gradient relevant to real membranes, the electrified system has the minimum number of excess charges (1 Cl^- shared between each of the outer salt-water baths): Only one of the two outer baths started with an excess Cl^- in the initial configuration. Figure 2(a) shows that this single excess Cl^- samples both periodically-connected outer water-baths sufficiently. The overall shape of the potential profiles is consistent with previously published results.[46] Figure 2(b) shows the temporal build-up of the potential profile from the electrified simulation, starting from the initial configuration and proceeding through the first 10 ps, 1 ns, and the full 10 ns. Data has been averaged over the two bilayers in order to take full advantage of the doubled sampling available from this system configuration. The overall shape of the potential profile equilibrates rapidly (on the order of several ps, only a few thousand timesteps). Within the lipid region, the equilibration period is a bit longer, but is still only on the order of nanoseconds. The potential drop of 170 mV is somewhat lower than that predicted (see Methods), but we believe this difference to be a minor one that partially reflects the uncertainty in the simulated membrane capacitance. Additionally, the potential profile for the neutral simulation shows a small non-zero gradient, which most likely reflects finite size-effects, and will be addressed in future reports.

By integrating the total charge density, Fig. 3 shows the asymmetric build-up of charge in the interfacial region of the outer and inner monolayers. As would be predicted based upon the direction of the electric field, there is an excess of negative charge at the outer monolayer and an excess of positive charge at the inner monolayer, inside of the two carbonyl distributions (18 Å$<z<$46 Å; note the bilayer center is at $z=30$ Å). The two curves are nearly identical in the salt-water baths, but the electrified curve becomes more negative at $z\approx18$ Å and then more positive at $z\approx40$ Å. The locations of these two transitions are thus shifted by approximately 2 Å, which may reflect a difference in penetration depth of the Cl^- and Na^+.[10–12,14] In addition to affecting the overall charge distribution, the electric field also affects the distributions of individual lipid chemical groups (not shown). Specifically, in the electrified simulation the inner leaflet distributions tend to be sharper and narrower than those of the outer leaflets. This phenomenon is not observed in the neutral case, in which the distributions are symmetric in all monolayer leaflets. Such differences in the molecular distributions at the outer and inner monolayers, in addition to those shown in Fig. 3, confirm that the statistical sampling of the charge imbalance is enough to impact the overall equilibrated charge distribution.

In conclusion, we have shown that current computational resources are sufficient for simulating an explicit and biologically relevant transmembrane potential. Specifically, simulations with a central unit cell consisting of two bilayers separating three salt-water baths avoid the periodicity problem. While these simulations are by necessity quite large, we show here that they should now be considered an option, and may be used to complement and evaluate more tractable approaches including continuum models and applied electric fields. We have shown that even on a short time-scale (10 ns in this case) the dynamic sampling of the charge imbalance clearly affects the overall charge distribution, consistent with the direction of the electric field. Additionally, we have presented a new derivation of the double integral equation for this periodic geometry that should be used in future applications of this method. All-atom simulations such as those presented here achieve a level of detail which can in the future be used to evaluate the specific role of water and salt ions in establishing the electric field, and to parse local and global effects on the lipids. Ongoing simulations will address the effect of the potential gradient on the dynamics of lipid components, specifically the headgroup and chain order parameters.

ACKNOWLEDGMENTS

The authors wish to thank Dr. Horia I. Petrache for an initial DMPC multilayer, and Anastasia Gentilcore for help with the computation. J.N.S. was partially funded by the Whitaker Foundation and an NIH NRSA grant. Sandia is a multiprogram laboratory operated by Sandia Corporation, a

Lockheed Martin Company for the United States Department of Energy's National Nuclear Security Administration under contract DE-AC04-94AL85000.

[1] Y. Zhou and R. MacKinnon, Biochem. J. **43**, 4978 (2004).
[2] B. Hille, *Ionic Channels of Excitable Membranes* (Sinauer, Sunderland, 1992).
[3] R. B. Gennis, *Biomembranes: Molecular Structure and Function* (Springer-Verlag, 1989).
[4] R. J. Clarke, Adv. Colloid Interface Sci. **89–90**, 263 (2001).
[5] E. Neher and B. Sakmann, Nature (London) **260**, 799 (1976).
[6] S. McLaughlin, Annu. Rev. Biophys. Biophys. Chem. **18**, 113 (1989).
[7] J. D. Faraldo-Gomez and B. Roux, J. Mol. Biol. **339**, 981 (2004).
[8] S. Berneche and B. Roux, Nature (London) **414**, 73 (2001).
[9] I. H. Shrivastava and M. S. P. Sansom, Eur. Biophys. J. Biophys. Lett. **31**, 207 (2002).
[10] J. N. Sachs and T. B. Woolf, J. Am. Chem. Soc. **125**, 8742 (2003).
[11] R. A. Bockmann, A. Hac, T. Heimburg, and H. Grubmuller, Biophys. J. **85**, 1647 (2003).
[12] S. A. Pandit, D. Bostick, and M. L. Berkowitz, Biophys. J. **84**, 3742 (2003).
[13] P. Mukhopadhyay, L. Monticelli, and D. P. Tieleman, Biophys. J. **86**, 1601 (2004).
[14] J. N. Sachs, H. Nanda, H. I. Petrache, and T. B. Woolf, Biophys. J. **86**, 3772 (2004).
[15] B. Roux, Biophys. J. **73**, 2980 (1997).
[16] B. Roux, Biophys. J. **77**, 139 (1999).
[17] D. P. Tieleman, H. J. C. Berendsen, and M. S. P. Sansom, Biophys. J. **80**, 331 (2001).
[18] A. Suenaga, Y. Komeji, M. Uebayasi, T. Meguro, M. Saito, and I. Yamato, Biosci. Rep. **18**, 39 (1998).
[19] G. S. Del Buono, T. S. Cohen, and P. J. Rossky, J. Mol. Liq. **60**, 221 (1994).
[20] J. E. Roberts and J. J. Schnitker, Chem. Phys. **102**, 450 (1995).
[21] S. G. Kalko, G. Sese, and J. A. Padro, J. Chem. Phys. **104**, 9578 (1996).
[22] C. Sagui and T. A. Darden, Annu. Rev. Biophys. Biomol. Struct. **28**, 155 (1999).
[23] L. Perera, U. Essmann, and M. L. Berkowitz, Langmuir **12**, 2625 (1996).
[24] J. N. Glosli and M. R. Philpott, Electrochim. Acta **41**, 2145 (1996).
[25] E. Spohr, J. Chem. Phys. **107**, 6342 (1997).
[26] I. C. Yeh and M. L. Berkowitz, J. Chem. Phys. **111**, 3155 (1999).
[27] P. S. Crozier, R. L. Rowley, E. Spohr, and D. J. Henderson, Chem. Phys. **112**, 9253 (2000).
[28] D. E. Parry, Surf. Sci. **49**, 433 (1975).
[29] D. M. Heyes, M. Barber, and J. H. R. Clarke, J. Chem. Soc., Faraday Trans. 2 **73**, 1485 (1977).
[30] S. W. de Leeuw and J. W. Perram, Mol. Phys. **37**, 1313 (1979).
[31] S. Y. Liem and J. H. R. Clarke, Mol. Phys. **92**, 19 (1997).
[32] A. H. Widmann and D. B. Adolf, Comput. Phys. Commun. **107**, 167 (1997).
[33] J. N. Sachs, H. I. Petrache, D. M. Zuckerman, and T. B. Woolf, J. Chem. Phys. **118**, 1957 (2003).
[34] D. Bostick and M. L. Berkowitz, Biophys. J. **85**, 97 (2003).
[35] J. Dzubiella, R. J. Allen, and J. P. Hansen, J. Chem. Phys. **120**, 5001 (2004).
[36] B. R. Brooks, R. E. Bruccoleri, B. D. Olafson, D. J. States, S. Swaminathan, and M. Karplus, J. Comp. Chem. **4**, 187 (1983).
[37] H. I. Petrache, S. Tristram-Nagle, and J. F. Nagle, Chem. Phys. Lipids **95**, 83 (1998).
[38] http://www.pharmacy.umaryland.edu/faculty/amackere/force_fields.htm/par_all22_prot.inp
[39] A. D. MacKerell, Jr., D. Bashford, M. Bellott *et al.*, J. Phys. Chem. B **102**, 3586 (1998).
[40] http://www.cs.sandia.gov/~sjplimp/lammps.html
[41] S. J. Plimpton, J. Comput. Phys. **117**, 1 (1995).
[42] S. J. Plimpton, R. Pollock, and M. Stevens, *Particle-Mesh Ewald and rRESPA for Parallel Molecular Dynamics Simulations*, in Proceedings of the Eighth SIAM Conference on Parallel Processing for Scientific Computing, Minneapolis, MN, March 1997.
[43] M. Deserno and C. J. Holm, J. Chem. Phys. **109**, 7678 (1998).
[44] M. Deserno and C. J. Holm, J. Chem. Phys. **109**, 7694 (1998).
[45] http://www.cs.sandia.gov/cplant/
[46] L. Saiz and M. L. Klein, J. Chem. Phys. **116**, 3052 (2002).